

Network analysis for the steady-state thermodynamic uncertainty relation

Yasuhiro Utsumi

*Department of Electrical and Electronic Engineering,
Faculty of Engineering, Mie University, Tsu, 514-8507, Mie, Japan.*

(Dated: May 7, 2024)

We perform network analysis of a system described by the master equation to estimate the lower bound of the steady-state current noise, starting from the level 2.5 large deviation function and using the graph theory approach. When the transition rates are uniform, and the system is driven to a non-equilibrium steady state by unidirectional transitions, we derive a noise lower bound, which accounts for fluctuations of sojourn times at all states and is expressed using mesh currents. This bound is applied to the uncertainty in the signal-to-noise ratio of the fluctuating computation time of a schematic Brownian computation plus reset process described by a graph containing one cycle. Unlike the mixed and pseudo-entropy bounds that increase logarithmically with the length of the intended computation path, this bound depends on the number of extraneous predecessors and thus captures the logical irreversibility.

I. INTRODUCTION

The thermodynamic uncertainty relation (TUR) provides a universal trade-off between precision and dissipation [1]. In the last decade, the TUR and its relatives—the trade-off relation and speed limits—have been discussed from various perspectives, e.g., Ref. [2]. Among these, the TUR has been applied to Bayes nets [3] and Brownian computation models [4]. Such networks, typically large-scale, possess information processing capabilities, making them intriguing subjects from novel aspects of the thermodynamics of computation [5, 6]. However, the TUR bound is anticipated to be weak for large networks because it is formulated in quantities, such as entropy production and activities, that increase as the system size grows. Therefore, tightening the bound is necessary for the practical application of TUR to computation models extended to include dynamics.

Graph theory is a well-established tool for analyzing electric circuit networks [7–10]. The network is algebraically treated using the circuit matrices, i.e., the incidence matrix, the cycle (loop) matrix, and the cut-set matrix. This approach aims to systematically reduce the number of free coordinates in the circuit equations or Lagrangians [10]. In the present paper, we perform a network analysis of a directed multigraph describing a Markov chain in the steady state. Such a graph can describe the Brownian computation plus reset process [4, 11].

For this purpose, we go back to the level 2.5 large deviation function adopted in early TUR studies [12–20]. The level 2.5 large deviation function provides the joint probability distribution of the numbers of jumps at all arcs and the sojourn times at all nodes in the limit of long measurement time. It derives a formally exact expression of the probability distribution of steady-state current, thus serving as a solid starting point for the network analysis. We derive a lower bound of the current noise when considering both bidirectional and unidirectional transition processes with uniform transition rates. The importance of network topology has been recognized

in the studies of the steady-state TUR [16–18] and the level 2.5 large deviation theory [12, 13] in connection to the steady-state fluctuation theorem [21]. These studies have focused on the universal aspect, while in the present paper, we emphasize practical application to large networks, especially to the Brownian computation model.

A secondary purpose of the paper is to provide an elementary derivation of the level 2.5 large deviation function based on the full-counting statistics (FCS) [22, 23]. The original derivation is rigorous and intricate [12, 13]. We aim for our derivation to be an accessible introduction to this concept for the mesoscopic quantum transport community and to make this paper self-contained simultaneously.

The structure of the paper is as follows: In Sec. II, we re-derive the level 2.5 large deviation function using the FCS approach and summarize previously known noise lower bounds. This section also introduces notations, which we use for our graph theoretical analysis. Section III explains our contributions: After introducing the circuit matrices, we derive a lower bound of current noise by duality transformation for systems with uniform transition rates. In Sec. IV, we apply our bound to a schematic Brownian computation model. Section V summarizes our results.

II. LEVEL 2.5 RATE FUNCTION AND TUR

A. FCS approach

The state transition diagram of a continuous-time Markov chain is a directed multigraph $G_m = (V, E_m)$, where the set of nodes V and the set of arcs (directed edges) E_m represent states and transitions, respectively. We focus on a connected graph with a unique steady state for simplicity. The direction of an arc corresponds to the direction of a transition. We write the arc $e \in E_m$ from the tail node $v_+ \in V$ to the head node $v_- \in V$ as a tuple $e = (v_- \leftarrow v_+)$. The boundary operator ∂^\pm maps the arc to the node as $\partial^\pm e = v_\pm$. The positive (negative) inci-

dence matrix is defined as, $D_{v,e}^\pm = \delta_{v,\partial^\pm e}$. The incidence matrix is $D = D^+ - D^-$. We denote the reversed arc of e as $-e = (v_+ \leftarrow v_-)$, which satisfies, $D_{v,-e}^\pm = D_{v,e}^\mp$. The master equation is,

$$\dot{n}_v = - \sum_{e \in E_m} D_{v,e} a_e(n_v), \quad (1)$$

$$a_e(n_v) = \sum_{v \in V} \Gamma_e D_{v,e}^+ n_v = \Gamma_e n_{\partial^+ e}, \quad (2)$$

where n_v is the state probability of node $v \in V$, and $\Gamma_e > 0$ is the transition rate associated to arc e .

We introduce the number of transitions through each arc e in its direction, W_e , and the sojourn time at each node v , τ_v . Their joint probability distribution function during the measurement time τ is,

$$\mathcal{P}_\tau(\{W_e\}, \{\tau_v\}) = \int \prod_{e \in E_m} \frac{d\lambda_e}{2\pi} \prod_{v \in V} \frac{d\xi_v}{2\pi} \mathcal{Z}_\tau(\{i\lambda_e\}, \{i\xi_v\}) \times e^{-i \sum_{e \in E_m} \lambda_e W_e - i \sum_{v \in V} \xi_v \tau_v}, \quad (3)$$

where λ_e and ξ_v are the counting fields for currents [22] and dwell times [23]. In the limit of long measurement time τ , $\mathcal{Z}_\tau(\{i\lambda_e\}, \{i\xi_v\}) \approx e^{\tau \Lambda(\{i\lambda_e\}, \{i\xi_v\})}$, where $\Lambda(\{i\lambda_e\}, \{i\xi_v\})$ is the eigenvalue of the modified (tilted) transition rate matrix,

$$L_{v,v'} = \sum_{e \in E_m} \Gamma_e \left(D_{v,e}^- e^{i\lambda_e} D_{v',e}^+ - D_{v,e}^+ D_{v',e}^+ \right) + i\xi_v \delta_{v,v'}, \quad (4)$$

with the maximum real part. Then, within the saddle point approximation, $\ln \mathcal{P}_\tau(\{W_e\}, \{\tau_v\}) \approx \tau \mathcal{I}(\{w_e\}, \{n_v\})$, where the rate function is,

$$\mathcal{I}(\{w_e\}, \{n_v\}) = \sup_{x_e, y_v \in \mathbb{R}} \left(\Lambda(\{x_e\}, \{y_v\}) - \sum_{e \in E_m} x_e w_e - \sum_{v \in V} y_v n_v \right). \quad (5)$$

The flux $w_e = W_e/\tau$ and the node state probability $n_v = \tau_v/\tau$ satisfy the Kirchhoff current law (KCL) and the normalization condition, respectively:

$$\sum_{e \in E_m} D_{v,e} w_e = 0, \quad (6)$$

$$\sum_{v \in V} n_v = 1, \quad (0 \leq n_v \leq 1). \quad (7)$$

We introduce the orthonormalized right and left eigenvectors associated with the eigenvalue Λ as,

$$\sum_{v' \in V} L_{v,v'} u_{v'}^R = \Lambda u_v^R, \quad \sum_{v \in V} u_v^L L_{v,v'} = u_{v'}^L \Lambda. \quad (8)$$

By noticing that u_v^L and u_v^R are orthonormalized and are the functions of x_e and y_v , the change

of eigenvalue induced by small variations δx_e and δy_v is calculated as, $\delta \Lambda = \sum_{v,v' \in V} u_v^L \delta L_{v,v'} u_{v'}^R = \sum_{e \in E_m} \delta x_e \Gamma_e e^{x_e} u_{\partial^- e}^L u_{\partial^+ e}^R + \sum_{v \in V} \delta y_v u_v^L u_v^R$. By using this we find that the maximum in Eq. (5) is achieved when x_e and y_v implicitly fulfill,

$$n_v = u_v^L u_v^R, \quad x_e = \ln \frac{w_e}{a_e(n_v)} + \sum_{v \in V} D_{v,e} \ln u_v^L. \quad (9)$$

By substituting these solutions into Eq. (5) and using the KCL (6), we obtain the level 2.5 large deviation function:

$$\mathcal{I}(\{w_e\}, \{n_v\}) = \sum_{e \in E_m} a_e(n_v) \psi \left(\frac{w_e}{a_e(n_v)} \right), \quad (10)$$

$$\psi(x) = x - 1 - x \ln x. \quad (11)$$

B. Bidirectional and unidirectional processes

The set of arcs is partitioned into mutually disjoint sets of arcs for unidirectional transitions $E_{\text{uni}} = \{e | e \in E_m \wedge -e \notin E_m\}$ and bidirectional transitions $E_{\text{bi}} = \{e | e \in E_m \wedge -e \in E_m\}$ as $E_m = E_{\text{uni}} \cup E_{\text{bi}}$ and $E_{\text{uni}} \cap E_{\text{bi}} = \emptyset$. The set for bidirectional transitions is further partitioned into the sets for forward transitions E_b and backward transitions \overline{E}_b as $E_{\text{bi}} = E_b \cup \overline{E}_b$ and $E_b \cap \overline{E}_b = \emptyset$. Here and hereafter, we use the overline to represent the set of reversed arcs, $\overline{A} = \{-e | e \in A\}$. In the following, we limit ourselves to the case that there exists E_b so that an oriented graph $G = (V, E = E_{\text{uni}} \cup E_b)$ contains a directed rooted spanning tree, $T = (V(T) = V, E(T))$. For $e \in E_b$, we introduce anti-symmetrized and symmetrized fluxes, $j_e = w_e - w_{-e}$ and $g_e = w_e + w_{-e}$, and integrate out the latter,

$$\sum_{e \in E_b} \sup_{g_e \in \mathbb{R}} \left(a_e \psi \left(\frac{g_e + j_e}{2a_e} \right) + a_{-e} \psi \left(\frac{g_e - j_e}{2a_{-e}} \right) \right). \quad (12)$$

This can be done (see e.g. Ref. [18]) and the result is,

$$\mathcal{I}(\{j_e\}, \{n_v\}) = \sum_{e \in E_b} 2\psi_{\text{bi}} \left(\frac{j_e}{2\sqrt{a_e a_{-e}}}, \frac{j_e(n_v)}{2\sqrt{a_e a_{-e}}} \right) \times \sqrt{a_e a_{-e}} + \sum_{e \in E_{\text{uni}}} a_e \psi \left(\frac{j_e}{a_e} \right), \quad (13)$$

$$\psi_{\text{bi}}(x, y) = \sqrt{1+x^2} - \sqrt{1+y^2} - x(\sinh^{-1} x - \sinh^{-1} y). \quad (14)$$

Here we write $j_e = w_e > 0$ for $e \in E_{\text{uni}}$ and introduced, $j_e(n_v) = a_e(n_v) - a_{-e}(n_v)$. The KCL (6) for the edge current becomes,

$$\sum_{e \in E} D_{v,e} j_e = 0. \quad (15)$$

The steady-state edge current $j_e(n_v^{\text{st}})$, where n_v^{st} is the node state probability in the steady-state, satisfies the

KCL. The rate function (13) takes the maximum at $j_e = j_e(n_v^{\text{st}})$ and $n_v = n_v^{\text{st}}$ as $\mathcal{I}(\{j_e(n_v^{\text{st}})\}, \{n_v^{\text{st}}\}) = 0$.

The node state probabilities in the steady state can be calculated using Kirchhoff-Hill theorem [24–26]:

$$n_v^{\text{st}} = \frac{1}{Z} \sum_{\mu=1}^{M_v} \prod_{e \in E(T_v^\mu(G))} \Gamma_e. \quad (16)$$

Here $T_v^\mu(G)$ ($\mu = 1, \dots, M_v$) is the v -directed spanning tree and Z is the normalization constant. M_v is the number of distinct v -directed spanning trees.

C. Mixed and pseudo-entropy bounds

We are interested in the probability distribution of the weighted sum of the edge currents,

$$w = \sum_{e \in E} d_e j_e, \quad (d_e \in \mathbb{R}), \quad (17)$$

which is obtained by contraction,

$$\tau^{-1} \ln \mathcal{P}_\tau(w) = \mathcal{I}(w) = \sup_{j_e \in \mathbb{R}, n_v \in [0,1]} \mathcal{I}(\{j_e\}, \{n_v\}), \quad (18)$$

subjected to the constraints (7), (15) and (17). The rate function $\mathcal{I}(w)$ takes the maximum at the average $\langle\langle w \rangle\rangle = \sum_{e \in E} d_e j_e(n_v^{\text{st}})$.

We introduce a parameter representing the deviation from the average, $\epsilon = w/\langle\langle w \rangle\rangle - 1$. Then by substituting $n_v = n_v^{\text{st}}$ and $j_e = j_e(n_v^{\text{st}})(\epsilon + 1)$ to Eq. (18) and by using the inequalities $\psi_{\text{bi}}(x, y) \geq -(x - y)^2 (\sinh^{-1} y)/(2y)$ [15], and (Appendix A),

$$\psi(x) \geq -\frac{(x-1)^2}{2} + \frac{(x-1)^3}{6} - \frac{(x-1)^4}{3}, \quad (19)$$

we obtain the mixed bound [27, 28]:

$$\mathcal{I}(w) \geq -\frac{\epsilon^2}{2} \Sigma_{\text{mix}} + \sum_{e \in E_{\text{uni}}} a_e(n_v^{\text{st}}) \psi^{(3,4)}(w/\langle\langle w \rangle\rangle), \quad (20)$$

$$\Sigma_{\text{mix}} = \frac{1}{2} \sum_{e \in E_{\text{b}}} j_e(n_v^{\text{st}}) \ln \frac{a_e(n_v^{\text{st}})}{a_{-e}(n_v^{\text{st}})} + \sum_{e \in E_{\text{uni}}} a_e(n_v^{\text{st}}), \quad (21)$$

where $\psi^{(3,4)}$ is the cubic and quartic terms of the right-hand side of Eq. (19). Equation (20) applies to all cumulants.

In the following, we focus on the second cumulant and utilize edge current and state probability vectors for concise presentations. We refer to T^* as the cotree of T , which contains arcs not in T , $E(T) \cup E(T^*) = E$ and $E(T) \cap E(T^*) = \emptyset$. Hereafter, the number of elements of a set A is denoted as $|A|$. The edge current vector $\mathbf{j} = [\mathbf{j}_t \ \mathbf{j}_c]^T \in \mathbb{R}^{|E|}$ is an $|E|$ component real vector. Here $\mathbf{j}_t = [j_{t_1}, \dots, j_{t_{|E(T)|}}]^T$ and $\mathbf{j}_c = [j_{c_1}, \dots, j_{c_{|E(T^*)|}}]^T$ are defined on twigs (arcs of the

directed rooted spanning tree T) $t_1, \dots, t_{|E(T)|} \in E(T)$ and on chords (arcs of the cotree T^*) $c_1, \dots, c_{|E(T^*)|} \in E(T^*)$, respectively. The state probability vector $\mathbf{n} \in \mathbb{R}^{|V|}$ is $\mathbf{n} = [n_{v_1}, \dots, n_{v_{|V|}}]^T$, where, $v_1, \dots, v_{|V|} \in V$.

A small deviation $\epsilon \ll 1$ shifts the maximizing parameters as,

$$\mathbf{j} = \mathbf{j}(n_v^{\text{st}}) + \mathbf{j}^\perp \epsilon + \mathbf{j}^{(2)} \epsilon^2/2 + \dots, \quad (22)$$

$$\mathbf{n} = \mathbf{n}^{\text{st}} + \phi \epsilon + \mathbf{n}^{(2)} \epsilon^2/2 + \dots. \quad (23)$$

By substituting them into Eq. (18) and expanding up to second order in ϵ , we obtain, $\mathcal{I}(w) \approx -\epsilon^2 \langle\langle w \rangle\rangle^2 / (2 \langle\langle w^2 \rangle\rangle)$, where [29],

$$\frac{\langle\langle w \rangle\rangle^2}{\langle\langle w^2 \rangle\rangle} = \inf_{\mathbf{j}^\perp \in J^{(1)}, \phi \in P^{(1)}} (\mathbf{j}^\perp - \mathbf{j}(\phi))^T \mathbf{G}^{-1} (\mathbf{j}^\perp - \mathbf{j}(\phi)). \quad (24)$$

The inverse of diagonal weight matrix is $\mathbf{G} = \text{diag } \mathbf{g}(n_v^{\text{st}})$ and $g_e(n_v) = a_e(n_v) + a_{-e}(n_v)$. Here and hereafter, we set $\Gamma_{-e} = 0$ for $e \in E_{\text{uni}}$. The constraints (7), (15) and (17) are,

$$J^{(1)} = \left\{ \mathbf{j}^\perp \in \mathbb{R}^{|E|} \mid (\langle\langle w \rangle\rangle = \mathbf{d}^T \mathbf{j}^\perp) \wedge (\mathbf{j}^\perp \in \ker \mathbf{D}) \right\}, \quad (25)$$

$$P^{(1)} = \left\{ \phi \in \mathbb{R}^{|V|} \mid \mathbf{1}^T \phi = 0 \right\}, \quad (26)$$

where $\mathbf{d} \in \mathbb{R}^{|E|}$, $\mathbf{D} \in \mathbb{R}^{|V| \times |E|}$ and $\mathbf{1}$ is a real vector whose entries are 1s.

By setting $\phi = \mathbf{0}$ and $\mathbf{j}^\perp = \mathbf{j}(n_v^{\text{st}})$, Eq. (24) naturally leads to the pseudo-entropy bound [28]:

$$\frac{\langle\langle w \rangle\rangle^2}{\langle\langle w^2 \rangle\rangle} \leq \Sigma_{\text{pseudo}} = \sum_{e \in E} \frac{(j_e(n_v^{\text{st}}))^2}{\Gamma_e n_{\partial^+ e}^{\text{st}} + \Gamma_{-e} n_{\partial^- e}^{\text{st}}}. \quad (27)$$

Equation (24) is a quadratic optimization problem in $|E| + |V|$ parameters subjected to the constraints (25) and (26). On the other hand, Eqs. (21) and (27) imply that the bound depends on the length of cycles. In the following section, we will systematically reduce the number of free parameters.

III. LOWER BOUND OF CURRENT NOISE

A. Circuit matrices

We summarize circuit matrices relevant to our network analysis (see, e.g., Refs. [7, 8] and Appendices of Ref. [10]). We write a fundamental cycle C_{e_1} of length ℓ as a tuple, a sequence of one chord $e_1 \in E(T^*)$ and $\ell - 1$ twigs $e_2, e_3, \dots, e_\ell \in E(T)$ or reversed ones $e_2, e_3, \dots, e_\ell \in \overline{E(T)}$:

$$C_{e_1} = (e_\ell, \dots, e_3, e_2, e_1). \quad (28)$$

The head and tail of adjacent arcs, e_n and e_{n+1} , ($n = 1, \dots, \ell - 1$) share the same node $\partial^- e_n = \partial^+ e_{n+1}$. The first and last arcs satisfy the periodic boundary condition $\partial^- e_\ell = \partial^+ e_1$. The fundamental cycle matrix $\mathbf{B} \in \mathbb{R}^{|E(T^*)| \times |E|}$ indicates which arcs are included in each of $|E(T^*)|$ fundamental cycles:

$$\mathbf{B} = [-\mathbf{F}^T \quad \mathbf{I}_{|E(T^*)|}], \quad (29)$$

where $\mathbf{I}_{|E(T^*)|}$ is a $|E(T^*)| \times |E(T^*)|$ unit matrix and $\mathbf{F} \in \mathbb{R}^{|E(T)| \times |E(T^*)|}$,

$$(\mathbf{F})_{t,c} = \mathbb{1}_{C_c}(-t) - \mathbb{1}_{C_c}(t), \quad (30)$$

for $c \in E(T^*)$ and $t \in E(T)$. The indicator function $\mathbb{1}_A(a)$ equals 1 if $a \in A$ and equals 0 if $a \notin A$.

There is a unique directed path from the root v_0 to a node v along the directed rooted spanning tree T , which we write as a sequence of twigs $e_1, e_2, \dots, e_\ell \in E(T)$ as,

$$P_{v \leftarrow v_0} = (e_\ell, \dots, e_2, e_1). \quad (31)$$

Here ℓ is the length of the path. Similar to the cycle, the head and tail of adjacent arcs share the same node. The two endpoints are $\partial^+ e_1 = v_0$ and $\partial^- e_\ell = v$. We introduce a root-to-node path matrix $\mathbf{S} \in \mathbb{R}^{|V| \times |E(T)|}$ as a variant of the node-to-datum path matrix [7–9],

$$(\mathbf{S})_{v,t} = \mathbb{1}_{P_{v \leftarrow v_0}}(t), \quad (32)$$

which is 1(0) if a twig $t \in E(T)$ is in (not in) the path from the root v_0 to the node v . The fundamental cutset matrix $\mathbf{Q} \in \mathbb{R}^{|E(T)| \times |E|}$ is then introduced as (Appendix B),

$$-\mathbf{S}^T \mathbf{D} = \mathbf{Q} = [\mathbf{I}_{|E(T)|} \quad \mathbf{F}], \quad (33)$$

which implies that \mathbf{S} acts as the line integral along the directed rooted spanning tree. The fundamental cutset is a minimal set of arcs consisting of one twig and zero or more chords that is the boundary of two regions. Its (t, e) component is 1(−1) if an arc e is in the fundamental cutset with respect to the twig t and bridges the two regions in the same (opposite) direction of the twig t .

The incidence matrix and the cycle matrix satisfy (Appendix B),

$$\mathbf{D}\mathbf{B}^T = \mathbf{0}_{|V| \times |E(T^*)|}, \quad (34)$$

$$\mathbf{B}\mathbf{D}^T = \mathbf{0}_{|E(T^*)| \times |V|}, \quad (35)$$

where, for example, $\mathbf{0}_{|V| \times |E(T^*)|}$ is a $|V| \times |E(T^*)|$ zero matrix. The cutset matrix satisfies similar relations:

$$\mathbf{Q}\mathbf{B}^T = \mathbf{0}_{|E(T)| \times |E(T^*)|}, \quad (36)$$

$$\mathbf{B}\mathbf{Q}^T = \mathbf{0}_{|E(T^*)| \times |E(T)|}. \quad (37)$$

Equalities (34), (35), (36) and (37) indicates,

$$\text{im}\mathbf{B}^T \subseteq \ker \mathbf{D}, \ker \mathbf{Q}, \quad (38)$$

$$\text{im}\mathbf{D}^T, \text{im}\mathbf{Q}^T \subseteq \ker \mathbf{B}. \quad (39)$$

The first (second) inclusion relation corresponds to that between groups of (co)boundaries and (co)cycles [30]. Intuitively, Eqs. (35) and (37) correspond to $\text{curl}(\text{grad}) = 0$ in the vector analysis.

B. Duality transformation

In the following, we limit ourselves to the uniform transition rates,

$$\Gamma_e = \Gamma = 1, \quad (e \in E_m). \quad (40)$$

In this case, the unidirectional transitions drive the system out of equilibrium. In Eq. (24), $\mathbf{j}(\phi)$ can be separated into the ‘curl-free’ component $\mathbf{D}^T \phi \in \text{im}\mathbf{D}^T$ and the source term coming from the unidirectional transitions:

$$\mathbf{j}(\phi) = \mathbf{D}^T \phi + \mathbf{\Pi} \mathbf{D}^{-T} \phi, \quad \mathbf{\Pi} = \sum_{e \in E_{\text{uni}}} \mathbf{e}_e^T \mathbf{e}_e. \quad (41)$$

where $\mathbf{e}_e \in \mathbb{R}^{|E|}$ is a unit vector, $(\mathbf{e}_e)_{e'} = \delta_{e,e'}$. One can check $\phi = (\mathbf{1}^T / |V| - \mathbf{I}_{|V|}) \mathbf{S} \nu$, where $\nu \in \mathbb{R}^{|E(T)|}$, satisfies the constraint (26). By substituting it into Eq. (41), we obtain,

$$\mathbf{j}(\phi) = \mathbf{\Phi}^{-1} \mathbf{Q}^T \nu, \quad (42)$$

$$\mathbf{\Phi}^{-1} = \mathbf{I}_{|E|} + \sum_{e' \in E_{\text{uni}}} [\mathbf{e}_{e'} \mathbf{\Omega}_{e'}^T \quad \mathbf{0}_{|E| \times |E(T^*)|}], \quad (43)$$

where $\mathbf{\Omega}_e \in \mathbb{R}^{|E(T)|}$ is,

$$(\mathbf{\Omega}_e)_t = |V(T_{\partial^- t})| / |V| - \mathbb{1}_{P_{\partial^- e \leftarrow v_0}}(t). \quad (44)$$

Here, $T_{\partial^- t}$ is a subtree rooted at $\partial^- t$ obtained by cutting the directed rooted spanning tree T by removing the arc t . The number of nodes in this subtree is $|V(T_{\partial^- t})| = \sum_{v \in V} (\mathbf{S})_{v,t}$. For explicit form of $\mathbf{\Phi}$, see Appendix C.

We perform the duality transformation [31], which is in the present context, integrating out the ‘curl-free’ component $\mathbf{Q}^T \nu$ by introducing the auxiliary field $\mathbf{J} \in \mathbb{R}^{|E|}$ to Eq. (24) as,

$$\frac{\langle\langle w \rangle\rangle^2}{\langle\langle w^2 \rangle\rangle} = \inf_{j^\perp \in J^{(1)}(w)} \sup_{\nu \in \mathbb{R}^{|E(T)|}} \sup_{\mathbf{J} \in \mathbb{R}^{|E|}} \left(-(\mathbf{J} - \mathbf{G}^{-1}\mathbf{i})^T \mathbf{G} (\mathbf{J} - \mathbf{G}^{-1}\mathbf{i}) + \mathbf{i}^T \mathbf{G}^{-1}\mathbf{i} \right) \quad (45)$$

$$= \inf_{j^\perp \in J^{(1)}(w)} \sup_{\nu \in \mathbb{R}^{|E(T)|}} \sup_{\mathbf{J} \in \mathbb{R}^{|E|}} \left(-\mathbf{J}^T \mathbf{G} \mathbf{J} + 2\mathbf{J}^T \mathbf{j}^\perp - 2\mathbf{J}^T \Phi^{-1} \mathbf{Q}^T \nu \right), \quad (46)$$

where $\mathbf{i} = \mathbf{j}^\perp - \mathbf{j}(\phi)$. Equation (46) is equivalent to,

$$\frac{\langle\langle w \rangle\rangle^2}{\langle\langle w^2 \rangle\rangle} = \inf_{j^\perp \in J^{(1)}(w)} \sup_{\mathbf{J} \in \mathbb{R}^{|E|}} \left(-\mathbf{J}^T \mathbf{G} \mathbf{J} + 2\mathbf{J}^T \mathbf{j}^\perp \right), \quad (47)$$

subjected to the constraint, $\Phi^{-1T} \mathbf{J} \in \ker \mathbf{Q}$, imposed by the Lagrange multiplier vector ν . From Eq. (38), the replacement of $\Phi^{-1T} \mathbf{J}$ with $\mathbf{B}^T \mathbf{A} \in \text{im} \mathbf{B}^T$, where $\mathbf{A} \in \mathbb{R}^{|E(T^*)|}$ is the mesh current vector, leads to

$$\frac{\langle\langle w \rangle\rangle^2}{\langle\langle w^2 \rangle\rangle} \leq \inf_{j^\perp \in J^{(1)}} \sup_{\mathbf{A} \in \mathbb{R}^{|E(T^*)|}} \left(-\mathbf{A}^T \mathbf{G}_2 \mathbf{A} + 2\mathbf{A}^T \mathbf{B} \Phi \mathbf{j}^\perp \right), \quad (48)$$

$$\mathbf{G}_2 = \mathbf{B} \Phi \mathbf{G} \Phi^T \mathbf{B}^T. \quad (49)$$

We find the maximizing \mathbf{A} by solving $\mathbf{G}_2 \mathbf{A} = \mathbf{B} \Phi \mathbf{j}^\perp$. Then the right-hand side of Eq. (48) becomes,

$$\inf_{j^\perp \in J^{(1)}} \left(\mathbf{j}^\perp{}^T \Phi^T \mathbf{B}^T \mathbf{G}_2^{-1} \mathbf{B} \Phi \mathbf{j}^\perp \right). \quad (50)$$

The replacement of $\mathbf{j}^\perp \in \ker \mathbf{D}$ with $\mathbf{B}^T \mathbf{f} \in \text{im} \mathbf{B}^T$ leads to the main result of the paper, the lower-bound of current noise:

$$\frac{\langle\langle w \rangle\rangle^2}{\langle\langle w^2 \rangle\rangle} \leq \inf_{\mathbf{f} \in F(w)} \left(\mathbf{f}^T \mathbf{B} \Phi^T \mathbf{B}^T \mathbf{G}_2^{-1} \mathbf{B} \Phi \mathbf{B}^T \mathbf{f} \right), \quad (51)$$

$$F(w) = \left\{ \mathbf{f} \in \mathbb{R}^{|E(T^*)|} \mid \langle\langle w \rangle\rangle = \mathbf{d}^T \mathbf{B}^T \mathbf{f} \right\}. \quad (52)$$

Eventually, we reduce to a quadratic optimization problem in mesh currents f_c ($c \in E(T^*)$) subjected to a linear constraint. In contrast to the mixed and pseudo-entropy bounds obtained by fixing $\phi = \mathbf{0}$, this expression accounts for fluctuations of sojourn times at all nodes.

IV. APPLICATION: BROWNIAN COMPUTATION

We apply Eq. (51) to the Brownian computation process schematically depicted as tree graphs (see Fig.10 of Ref. [5]). Figures 1 (a) and (b) show such graphs whose nodes represent logical states. In each panel, the bottom nodes are possible input states, and the top node corresponds to the output state. The computation proceeds from bottom to top, and the branching represents the logical irreversibility. In each panel, solid arcs constitute a directed rooted spanning tree $T = (V, E(T))$. The computation starts from the start state, $v_0 = \mathbf{i}$,

which we take as the root, to the output state $v_\ell = \mathbf{f}$. There is an intended computation path with length ℓ , $v_0 \rightarrow v_1 \rightarrow \dots \rightarrow v_\ell$ [thick solid arcs in panels (a) and (b)],

$$P_{v_\ell \leftarrow v_0} = (t_\ell, t_{\ell-1} \dots, t_1), \quad (53)$$

where $t_d = (v_d \leftarrow v_{d-1})$. From each node on the intended computation path, a subtree T_d rooted at the node v_d grows [shaded parts in panel (a)]. The set of nodes is then $V = \cup_{d=0}^\ell V(T_d)$, where $V(T_0) = \{v_0\}$. The nodes, except for the roots of the subtrees, represent extraneous predecessors; leaf nodes are either possible input states [bottom nodes in panels (a) and (b)] or ‘garden-of-Eden’ states with no predecessors [hatched nodes in panel (b)] [5]. All solid arcs are for bidirectional processes:

$$E(T) = E_b = \{t_1, \dots, t_\ell\} \cup_{d=0}^\ell E(T_d), \quad (54)$$

where $E(T_0) = \emptyset$.

The dotted arc in each panel is a chord c representing the unidirectional reset process. The intended computation path and the reset path constitute a cycle:

$$C_c = (t_\ell, \dots, t_1, c). \quad (55)$$

The reset current is measured at the chord $d_e = \delta_{e,c}$. We assume that there is no other chord, i.e., $E(T^*) = E_{\text{uni}} = \{c\}$. Consequently, no free parameter exists in Eq. (51).

We focus on the signal-to-noise ratio (SNR) of the probability distribution of the computation time, which we define as the first passage time [4, 11], being upper bounded by TUR [4, 19, 20, 32]. The Fano factor of reset current and the SNR for W resets are related as, $S/N = \sqrt{W \langle\langle w \rangle\rangle / \langle\langle w^2 \rangle\rangle}$ [4].

From Eq. (51), the lower bound of the Fano factor is obtained as (Appendix D),

$$\begin{aligned} \frac{\langle\langle w^2 \rangle\rangle}{\langle\langle w \rangle\rangle} &\geq \sum_{d=0}^\ell (2\ell - 2d + 1) \left(\frac{\mathcal{N}_d}{\sum_{d=0}^\ell \mathcal{N}_d} \right)^2 \\ &+ \sum_{d=0}^\ell 2(\ell - d + 1) \sum_{e \in E(T_d)} \left(\frac{|V(T_{d-e})|}{\sum_{d=0}^\ell \mathcal{N}_d} \right)^2, \end{aligned} \quad (56)$$

where $\mathcal{N}_d = \sum_{d'=0}^d |V(T_{d'})|$ is monotonically increasing in d . The bound depends on the detailed structure of subtrees $T(v_d)$. In the following, we present analytic expressions for two examples.

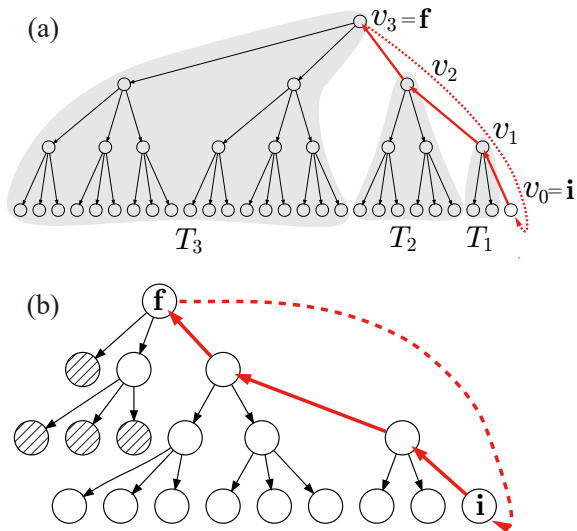


FIG. 1. Graphs for schematic Brownian computation plus reset process. Solid arcs constitute the directed rooted spanning tree rooted at $v_0 = i$, which is the start state. In each panel, thick solid arcs indicate the intended computation path from the start state $v_0 = i$ to the output state $v_\ell = f$. The dotted arc is the chord indicating the unidirectional reset process. In panel (a), shaded subtrees represent extraneous predecessors of the logical states at the root v_d ($d = 1, \dots, \ell$).

The first example is the model of Brownian logically reversible Turing machine (RTM) [4, 11], in which extraneous predecessors are absent, $|V(T_d)| = 1$ and $|V(T_{\partial-e})| = 0$ ($e \in E(T_d)$) for $d = 0, \dots, \ell - 1$. Then, $\mathcal{N}_d = d + 1$ and thus the right-hand side of Eq. (56) becomes,

$$\frac{2(1 + \tilde{\ell} + \tilde{\ell}^2)}{3\tilde{\ell}(1 + \tilde{\ell})}. \quad (57)$$

For $\ell \gg 1$, it approaches, $2/3$ as was obtained before [4].

The second example is the case where the directed rooted spanning tree forms a complete α -ary tree ($\alpha \geq 2$) if we reverse arcs of the intended computation path [Fig. 1 (a)]. This case, the right-hand side of Eq. (56) becomes (Appendix E),

$$\frac{\alpha(\alpha^{\tilde{\ell}} - 1)(4 + \alpha + \alpha^{\tilde{\ell}+1}) + \tilde{\ell}(\alpha - 1)(1 + \alpha + 4\alpha^{\tilde{\ell}+1})}{(\tilde{\ell}(1 - \alpha) + \alpha(\alpha^{\tilde{\ell}} - 1))^2}. \quad (58)$$

The lower bound approaches 1 for $\ell \gg 1$. This behavior is reminiscent of the SNR observed for the token-based Brownian circuit [4]. The weaker bound, which follows from Eq. (56),

$$\frac{\langle\langle w^2 \rangle\rangle}{\langle\langle w \rangle\rangle} \geq \sum_{d=0}^{\ell} \left(\frac{\mathcal{N}_d}{\sum_{d=0}^{\ell} \mathcal{N}_d} \right)^2, \quad (59)$$

explains this behavior: The right-hand side approaches 1 when the extraneous predecessors are concentrating on

the last subtree T_ℓ , $|V(T_\ell)| \approx |V|$. This condition is the case for the complete α -ary tree-like graph, $|V(T_\ell)|/|V| \approx 1 - 1/\alpha$ for $\ell \gg 1$.

Figure 2 shows the SNR for a single reset ($W = 1$) versus the length of the intended computation path ℓ . The top panel is for the Brownian RTM. The middle panel is for the complete 3-ary tree-like graph shown in Fig. 1 (a). In both panels, the analytic results, Eqs. (57) and (58) (solid lines) fit the numerical results (filled squares) obtained by the Gillespie algorithm. The SNR approaches $\sqrt{3}/2$ in the top panel, while in the middle panel, the SNR quickly approaches 1, i.e., the logical irreversibility degrades the SNR.

In each panel, filled circles and the dashed line indicate the mixed and pseudo-entropy bounds, Eqs. (21) and (27),

$$\begin{aligned} \frac{\Sigma_{\text{mix}}}{\langle\langle w \rangle\rangle} &= \sum_{d=0}^{\ell-1} \frac{1}{2} \ln \frac{n_d^{\text{st}}}{n_{d+1}^{\text{st}}} + 1 = \frac{1}{2} \ln \tilde{\ell} + 1, \quad (60) \\ \frac{\Sigma_{\text{pseudo}}}{\langle\langle w \rangle\rangle} &= \sum_{d=0}^{\ell} \frac{\langle\langle w \rangle\rangle}{2\ell - 2d + 1} = \ln 2 + \frac{1}{2} H_{\ell+1/2} \\ &\approx \ln 2 + \frac{\gamma}{2} + \frac{\ln \tilde{\ell}}{2}. \quad (61) \end{aligned}$$

Here H_n is the n -th harmonic number, and γ is the Euler's constant. Since the steady-state current only flows along the cycle, the entropy production depends only on the length of the intended computation path ℓ . It is independent of the number of the extraneous predecessors, which is large, e.g., there are $|V| - |C_c| = 3272$ extraneous states for the complete 3-ary tree-like graph with $\ell = 7$ corresponding to the middle panel of Fig. 2. From this respect, the mixed and pseudo-entropy bounds are considered tight. However, they fail to capture the logical irreversibility and become logarithmically weaker for the longer intended computation path.

The bottom panel of Fig. 2 corresponds to the 3-ary tree-like graph, Fig. 1 (b). The SNR is bigger than one and smaller than mixed and pseudo-entropy bounds. Note that the average computation time itself, which is the reciprocal of the average reset current $1/\langle\langle w \rangle\rangle = \sum_{d=0}^{\ell} (\ell - d + 1)|V(T_d)|/\Gamma$, increases with the number of extraneous states. We also note that the schematic Brownian computation models discussed here discard certain features of potential Brownian computation models: The token-based Brownian computation model [4] is concurrent and thus should contain many cycles in its graph. These cycles change the steady-state probabilities and alter the path-length dependence of mixed and pseudo-entropy bounds.

V. CONCLUSION

Starting from the level 2.5 large deviation function, we derive a lower bound of the Fano factor expressed

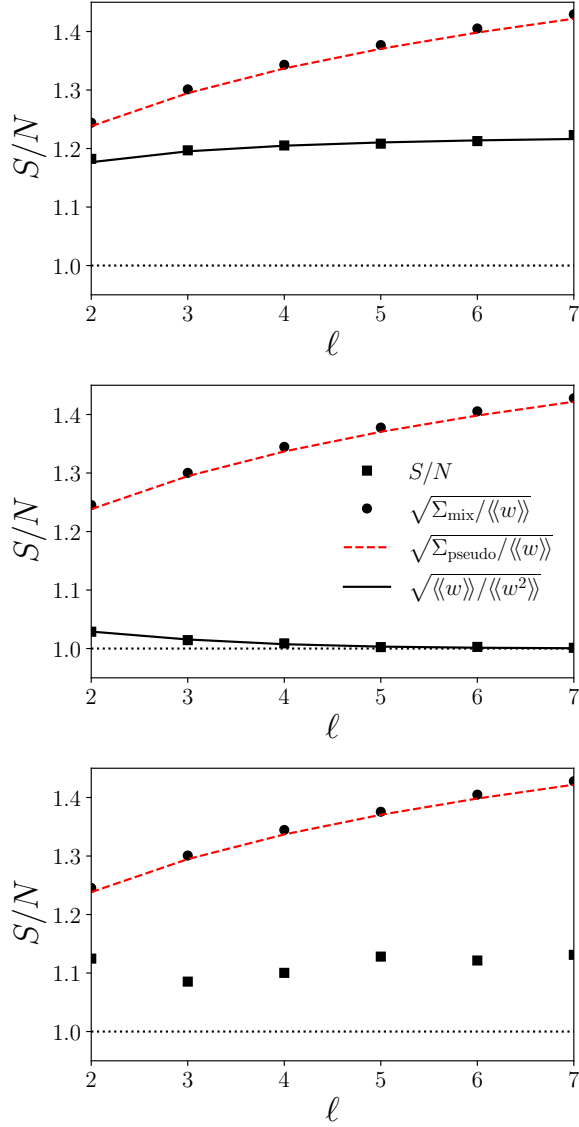


FIG. 2. Plots of the signal-to-noise ratio S/N versus the length of the intended computation path for (top) the Brownian RTM, (middle) the complete 3-ary tree-like graph, Fig. 1 (a), and (bottom) the full 3-ary tree-like graph, Fig. 1 (b). The results are for a single reset ($W = 1$). Filled squares are numerical results obtained by the Gillespie algorithm with 10^5 samples. The numerical results of the top and middle panels are fitted by the analytic solutions (solid lines). The mixed-bound (60) (filled circles) and the pseudo-entropy bound (61) (dashed line) are shown in all panels.

as a quadratic optimization problem in mesh currents subjected to a linear constraint. By the duality transformation and exploiting the root-to-node path matrix, we effectively integrate out fluctuations of sojourn times at all nodes when rates for bidirectional and unidirectional transitions are uniform. The bound applied to the schematic Brownian computation plus reset process shows that the logical irreversibility reduces the signal-

to-noise ratio of the fluctuating computation time. It is contrasted with the mixed and pseudo-entropy bounds, which are independent of the logical irreversibility and become weaker logarithmically in the length of the intended computation path.

ACKNOWLEDGMENTS

We thank Satoshi Nakajima for proving the inequality (19). This work was supported by JSPS KAKENHI Grants No. 18KK0385, No. 20H01827, No. 20H05666, and No. 24K00547, and JST, CREST Grant Number JPMJCR20C1, Japan.

Appendix A: Proof of the inequality (19)

Let us introduce a function,

$$f(x) = \psi(x) + \frac{(x-1)^2}{2} - \frac{(x-1)^3}{6} + \frac{(x-1)^4}{3}. \quad (\text{A1})$$

The first and second derivatives are,

$$f'(x) = -\ln x + \frac{(x-1)(8x^2 - 19x + 17)}{6}, \quad (\text{A2})$$

$$f''(x) = \frac{(x-1)^2(4x-1)}{x}. \quad (\text{A3})$$

Since, $f''(x) < 0$ for $0 < x < 1/4$ and $f''(x) \geq 0$ for $1/4 \leq x$, $f'(x)$ is monotonically decreasing for $0 < x < 1/4$ and weakly increasing for $1/4 \leq x$. The zeros of $f'(x)$ are $x = 1$ and $x = x^*$; Since $\lim_{x \rightarrow +0} f'(x) = \infty$ and $f'(1/4) = \ln 4 - 51/32 = -0.207 \dots < 0$, there exists x^* such that $0 < x^* < 1/4$ and $f'(x^*) = 0$. Then, $f'(x) \leq 0$ for $x^* \leq x \leq 1$, and $f'(x) > 0$ for $0 < x < x^*$ and $1 < x$. Therefore, a local maximum and a local minimum exist at $x = x^*$ and $x = 1$, respectively. Since $\lim_{x \rightarrow +0} f(x) = +0$ and the local minimum is $f(1) = 0$, we conclude $f(x) \geq 0$ for $x > 0$, which proves (19).

Appendix B: Proofs of Eqs. (33) and (34)

Equation (33) is calculated as, $(\mathbf{Q})_{t,e} = \mathbb{1}_{P_{\partial^- e \leftarrow v_0}}(t) - \mathbb{1}_{P_{\partial^+ e \leftarrow v_0}}(t)$. If $e \in E(T)$, it is 1 only when $t = e$ and 0 otherwise. If $e \in E(T^*)$, it is $-1(1)$, when $t(-t)$ is in the cycle C_e . Therefore,

$$(\mathbf{Q})_{t,e} = \begin{cases} \delta_{t,e} & (e \in E(T)) \\ \mathbb{1}_{C_e}(-t) - \mathbb{1}_{C_e}(t) = F_{t,e} & (e \in E(T^*)) \end{cases}, \quad (\text{B1})$$

which proves Eq. (33) [9].

We introduce δ^\pm , the dual of ∂^\pm , that maps V to E as, $\delta^\pm v = \{e | \partial^\pm e = v \wedge e \in E\}$. By using this, the incidence matrix is expressed as $(\mathbf{D}^\pm)_{v,e} = \mathbb{1}_{\delta^\pm v}(e)$. Then

$(\mathbf{D}^\pm \mathbf{B}^T)_{v,c}$ is calculated as,

$$(\mathbf{D}^\pm \mathbf{B}^T)_{v,c} = \sum_{e \in C_c} \mathbb{1}_{\delta^\pm v}(e), \quad (\text{B2})$$

if the cycle C_c goes along the directions of twigs of T , and

$$(\mathbf{D}^\pm \mathbf{B}^T)_{v,c} = \mathbb{1}_{\delta^\pm v}(c) - \sum_{t \in C_c - \{c\}} \mathbb{1}_{\delta^\pm v}(-t), \quad (\text{B3})$$

if C_c goes in the direction opposite to T . Here we write a path obtained from C_c by removing c as $C_c - \{c\}$. For both equations, (B2) and (B3), we obtain $(\mathbf{D}\mathbf{B}^T)_{v,c} = 0$, which proves Eq. (34).

Appendix C: Φ matrix

We write a unit vector as, $\mathbf{e}_e^T = [\mathbf{e}_e(T)^T \ \mathbf{e}_e(T^*)^T]$, where $\mathbf{e}_e(T) \in \mathbb{R}^{|E(T)|}$ and $\mathbf{e}_e(T^*) \in \mathbb{R}^{|E(T^*)|}$. Accordingly,

$$\begin{bmatrix} \Omega(T) \\ \Omega(T^*) \end{bmatrix} = \begin{bmatrix} \sum_{e' \in E_{\text{uni}} \cap E(T)} \mathbf{e}_{e'}(T) \Omega_{e'}^T \\ \sum_{e' \in E_{\text{uni}} \cap E(T^*)} \mathbf{e}_{e'}(T^*) \Omega_{e'}^T \end{bmatrix}. \quad (\text{C1})$$

By substituting them into Eq. (43), we obtain,

$$\Phi = \begin{bmatrix} (\mathbf{I}_{|E(T)|} + \Omega(T))^{-1} & \mathbf{0} \\ -\Omega(T^*) (\mathbf{I}_{|E(T)|} + \Omega(T))^{-1} & \mathbf{I}_{|E(T^*)|} \end{bmatrix}. \quad (\text{C2})$$

Appendix D: Derivations of Eq. (56)

By exploiting Eq. (16), the node state probability in the steady-state is,

$$n_v^{\text{st}} = (\ell - d + 1)/Z, \quad (v \in V(T_d)). \quad (\text{D1})$$

The $1 \times |E|$ cycle matrix is $B_{c,e} = 1_{C_c}(e)$. The nonzero components of $|E| \times |E|$ matrix Φ is $\Phi_{e,e} = 1$ for $e \in E$ and $\Phi_{c,t} = -|V(T_{\partial-t})|/|V|$ for $t \in E(T)$ and $c \in E(T^*)$ (Appendix C). The mesh current satisfying the constraint is $\mathbf{f} = \langle\langle w \rangle\rangle = \Gamma g_c$.

The number of node of subtree rooted at $\partial^- t_d$ is $|V(T_{\partial-t_d})| = \sum_{d'=d}^\ell |V(T_{d'})|$. By using this, we obtain,

$$\sum_{e \in C_c} \Phi_{e,t_d} = 1 - |V(T_{\partial-t_d})|/|V| = \mathcal{N}_{d-1}/|V|. \quad (\text{D2})$$

The relations mentioned above lead to,

$$\mathbf{B}\Phi\mathbf{B}^T = \sum_{d=1}^\ell \sum_{e \in C_c} \Phi_{e,t_d} + \mathbf{1} = \sum_{d=0}^\ell \frac{\mathcal{N}_d}{|V|}, \quad (\text{D3})$$

$$\begin{aligned} \frac{\mathbf{G}_2}{\langle\langle w \rangle\rangle} &= \sum_{d=1}^\ell \frac{g_{t_d}}{g_c} \left(\sum_{e' \in C_c} \Phi_{e',t_d} \right)^2 + \left(\sum_{e' \in C_c} \Phi_{e',c} \right)^2 \\ &+ \sum_{d=0}^\ell \sum_{e \in E(T_d)} \frac{g_e}{g_c} \left(\sum_{e' \in C_c} \Phi_{e',e} \right)^2 \end{aligned} \quad (\text{D4})$$

$$\begin{aligned} &= \sum_{d=0}^\ell (2\ell - 2d + 1) \left(\frac{\mathcal{N}_d}{|V|} \right)^2 + \sum_{d=0}^\ell 2(\ell - d + 1) \\ &\times \sum_{e \in E(T_d)} \left(\frac{|V(T_{\partial-e})|}{|V|} \right)^2, \end{aligned} \quad (\text{D5})$$

where we used $g_e/g_c = 2n_{v_d}^{\text{st}}/n_{v_e}^{\text{st}}$ and $\sum_{e' \in C_c} \Phi_{e',e} = \Phi_{c,e}$ for $e \in E(T_d)$. By combining Eqs. (D3) and (D5), the right-hand side of Eq. (56), $\mathbf{G}_2 \langle\langle w \rangle\rangle / (\mathbf{B}\Phi\mathbf{B}^T \mathbf{f})^2$ is obtained.

Appendix E: Derivations of Eq. (58)

Let $T(\alpha, h)$ a complete α -ary tree of height h . It contains $|V(T(\alpha, h))| = \sum_{h'=0}^h \alpha^{h'} = (\alpha^{h+1} - 1)/(\alpha - 1)$ nodes. In T_d , there are $N(T(\alpha, h)) = \alpha^{d-h-1}(\alpha - 1)$ ($h = 0, \dots, d-1$) such subtrees. Therefore,

$$|V(T_d)| = 1 + \sum_{h=0}^{d-1} N(T(\alpha, h)) = \alpha^d. \quad (\text{E1})$$

By exploiting these relations, we obtain,

$$\mathcal{N}_d = \frac{\alpha^{d+1} - 1}{\alpha - 1} \quad (\text{E2})$$

$$\sum_{d=0}^\ell \mathcal{N}_d = \frac{1 + \alpha^{\ell+2} + \ell - \alpha(\ell + 2)}{(\alpha - 1)^2}, \quad (\text{E3})$$

$$\begin{aligned} \sum_{e \in E(T_d)} |V(T_{\partial-e})|^2 &= \sum_{h=0}^{d-1} N(T(\alpha, h)) |V(T(\alpha, h))|^2 \\ &= \frac{\alpha^d [(1 + 2d)(1 - \alpha) + \alpha^{d+1}] - 1}{(\alpha - 1)^2}. \end{aligned} \quad (\text{E4})$$

By substituting them into the right-hand side of Eq. (56), we obtain Eq. (58).

-
- [1] J. M. Horowitz and T. R. Gingrich, Thermodynamic uncertainty relations constrain non-equilibrium fluctuations, *Nature Physics* **16**, 15 (2020).
- [2] N. Shiraishi, *An Introduction to Stochastic Thermodynamics: From Basic to Advanced* (Springer Nature Singapore, Singapore, 2023).
- [3] D. H. Wolpert, Uncertainty relations and fluctuation theorems for bayes nets, *Phys. Rev. Lett.* **125**, 200602 (2020).
- [4] Y. Utsumi, Y. Ito, D. Golubev, and F. Peper, Computation time and thermodynamic uncertainty relation of brownian circuits, (2022), arXiv:2205.10735 [cond-mat.stat-mech].
- [5] C. H. Bennett, The thermodynamics of computation—a review, *International Journal of Theoretical Physics* **21**, 905 (1982).
- [6] D. Wolpert, J. Korbelt, C. Lynn, F. Tasnim, J. Grochow, G. Kardeş, J. Aimone, V. Balasubramanian, E. de Giuli, D. Doty, N. Freitas, M. Marsili, T. E. Ouldrige, A. Richa, P. Riechers, Édgar Roldán, B. Rubenstein, Z. Toroczkai, and J. Paradiso, Is stochastic thermodynamics the key to understanding the energy costs of computation?, (2023), arXiv:2311.17166 [cond-mat.stat-mech].
- [7] P. Bryant, The algebra and topology of electrical networks, *Proceedings of the IEE - Part C: Monographs* **108**, 215 (1961).
- [8] F. Branin, Computer methods of network analysis, *Proceedings of the IEEE* **55**, 1787 (1967).
- [9] H. Takahashi, *Theory of Linear Lumped Parameter System I*, *Kisokougaku*, Iwanami kouza No. 6 (Iwanami shoten, Tokyo, 1969).
- [10] S. Rasmussen, K. Christensen, S. Pedersen, L. Kristensen, T. Bækkegaard, N. Loft, and N. Zinner, Superconducting circuit companion—an introduction with worked examples, *PRX Quantum* **2**, 040204 (2021).
- [11] Y. Utsumi, D. Golubev, and F. Peper, Thermodynamic cost of brownian computers in the stochastic thermodynamics of resetting, *The European Physical Journal Special Topics* **232**, 3259 (2023).
- [12] L. Bertini, A. Faggionato, and D. Gabrielli, Large deviations of the empirical flow for continuous time Markov chains, *Annales de l'Institut Henri Poincaré, Probabilités et Statistiques* **51**, 867 (2015).
- [13] L. Bertini, A. Faggionato, and D. Gabrielli, Flows, currents, and cycles for markov chains: Large deviation asymptotics, *Stochastic Processes and their Applications* **125**, 2786 (2015).
- [14] A. C. Barato and R. Chetrite, A formal view on level 2.5 large deviations and fluctuation relations, *Journal of Statistical Physics* **160**, 1154 (2015).
- [15] T. R. Gingrich, J. M. Horowitz, N. Perunov, and J. L. England, Dissipation bounds all steady-state current fluctuations, *Phys. Rev. Lett.* **116**, 120601 (2016).
- [16] P. Pietzonka, A. C. Barato, and U. Seifert, Affinity- and topology-dependent bound on current fluctuations, *Journal of Physics A: Mathematical and Theoretical* **49**, 34LT01 (2016).
- [17] M. Poletini, A. Lazarescu, and M. Esposito, Tightening the uncertainty principle for stochastic currents, *Phys. Rev. E* **94**, 052104 (2016).
- [18] T. R. Gingrich, G. M. Rotskoff, and J. M. Horowitz, Inferring dissipation from current fluctuations, *Journal of Physics A: Mathematical and Theoretical* **50**, 184004 (2017).
- [19] T. R. Gingrich and J. M. Horowitz, Fundamental bounds on first passage time fluctuations for currents, *Phys. Rev. Lett.* **119**, 170601 (2017).
- [20] J. P. Garrahan, Simple bounds on fluctuations and uncertainty relations for first-passage times of counting observables, *Phys. Rev. E* **95**, 032134 (2017).
- [21] D. Andrieux and P. Gaspard, Fluctuation theorem for currents and schnakenberg network theory, *Journal of Statistical Physics* **127**, 107 (2007).
- [22] D. A. Bagrets and Y. V. Nazarov, Full counting statistics of charge transfer in coulomb blockade systems, *Phys. Rev. B* **67**, 085316 (2003).
- [23] Y. Utsumi, Full counting statistics for the number of electrons in a quantum dot, *Phys. Rev. B* **75**, 035333 (2007).
- [24] T. L. Hill, Studies in irreversible thermodynamics iv. diagrammatic representation of steady state fluxes for unimolecular systems, *Journal of Theoretical Biology* **10**, 442 (1966).
- [25] J. Schnakenberg, Network theory of microscopic and macroscopic behavior of master equation systems, Re1978v. *Mod. Phys.* **48**, 571 (1976).
- [26] W. Weidlich, On the structure of exact solutions of discrete masterequations, *Zeitschrift für Physik B Condensed Matter* **30**, 345 (1978).
- [27] A. Pal, S. Reuveni, and S. Rahav, Thermodynamic uncertainty relation for systems with unidirectional transitions, *Phys. Rev. Res.* **3**, 013273 (2021).
- [28] N. Shiraishi, Optimal thermodynamic uncertainty relation in markov jump processes, *Journal of Statistical Physics* **185**, 19 (2021).
- [29] A. C. Barato, R. Chetrite, A. Faggionato, and D. Gabrielli, Bounds on current fluctuations in periodically driven systems, *New Journal of Physics* **20**, 103023 (2018).
- [30] P. W. Gross and P. R. Kotiuga, *Electromagnetic theory and computation: a topological approach*, *Mathematical Sciences Research Institute Publications*, Vol. 48 (Cambridge University Press, Cambridge, 2004).
- [31] N. Nagaosa, Problems related to superconductivity, in *Quantum Field Theory in Condensed Matter Physics* (Springer Berlin Heidelberg, Berlin, Heidelberg, 1999) pp. 113–160.
- [32] A. Pal, S. Reuveni, and S. Rahav, Thermodynamic uncertainty relation for first-passage times on markov chains, *Phys. Rev. Res.* **3**, L032034 (2021).